Kato *et al.*
Progress in Earth and Planetary Science (2023) 10:13
https://doi.org/10.1186/s40645-023-00543-5

Progress in Earth and Planetary Science

METHODOLOGY

Open Access

A simple method for taxon-specific purification of diatom frustules from ocean sediments using a cell sorter

Yuji Kato[1,2*], Yuki Morono[3], Akira Ijiri[3,4], Takeshi Terada[5] and Minoru Ikehara[2]

Abstract

It is necessary to purify diatom frustules by taxon to perform accurate geochemical analyses of diatom fossils preserved in sediments. However, the small size of diatoms has hitherto prevented taxon-specific purification; therefore, previous geochemical analyses of diatom frustules have been performed with mixtures of various taxa. In this study, we developed a taxon-selective collection method of diatom fossils that uses a cell sorter. The experimental material comprised six samples from a sediment core of Hole U1538A in the Scotia Sea, Atlantic sector of the Southern Ocean drilled during the International Ocean Discovery Program Expedition 382. Following conventional pretreatments (removal of organic matter and carbonates as well as clay minerals), we conducted cell sorter experiments focusing on the optical and fluorescence characteristics of the diatom fossils. We succeeded in selectively isolating with high purity five diatom taxa representing the Southern Ocean diatom flora: (1) discoid diatoms (mainly *Thalassiosira*) with a moderate degree of fluorescence; (2) *Fragilariopsis* (mainly *Fragilariopsis kerguelensis*), which exhibits the highest fluorescence values; (3) *Rhizosolenia*; (4) *Eucampia antarctica*; and (5) needle-shaped diatoms (*Thalassiothrix*). This taxon-specific diatom purification method will enable more accurate geochemical analyses, such as the oxygen isotope ratio ($\delta^{18}O$) of diatom frustules, which is likely to lead to significant advances in paleoceanography, especially at high latitudes or in upwelling zones where diatoms are abundant. This method will also be useful in paleolimnology, ocean biology, and phycology.

Keywords Diatom, Cell sorter, Microfossil, Sediment, Southern Ocean, International Ocean Discovery Program

1 Introduction

Fossil diatoms are important paleoenvironmental indicators, and many paleoceanographic studies have been carried out using their assemblage compositions (e.g., Smol and Stoermer 2010). In addition to assemblage-based studies, a considerable number of geochemical studies using diatom frustules (e.g., of oxygen isotope composition [$\delta^{18}O$]) have been conducted over the last few decades. In general, calcareous microfossils are rare or almost barren in high-latitude oceans (Dutkiewicz et al. 2016); therefore, $\delta^{18}O$ data of diatom frustules have been regarded as an important alternative paleoenvironmental indicator to $\delta^{18}O$ of foraminiferal shells (Labeyrie 1974; Juillet-Leclerc and Labeyrie 1987; Shemesh et al. 1992, 1995, 2002; Hodell et al. 2001; Swann et al. 2006; Swann

*Correspondence:
Yuji Kato
kato.yuji.ge@u.tsukuba.ac.jp
[1] Present Address: Faculty of Life and Environmental Sciences, University of Tsukuba, Tsukuba, Ibaraki 305-8572, Japan
[2] Center for Advanced Marine Core Research, Kochi University, Nankoku, Kochi 783-8502, Japan
[3] Kochi Institute for Core Sample Research, Institute for Extra-Cutting-Edge Science and Technology Avant-Garde Research (X-Star), Japan Agency for Marine-Earth Science and Technology (JAMSTEC), Nankoku, Kochi 783-8502, Japan
[4] Graduate School of Maritime Sciences, Kobe University, Kobe, Hyogo 658-0022, Japan
[5] Marine Works Japan, Ltd., Yokosuka, Kanagawa 237-0063, Japan

and Leng 2009). Other examples of geochemical studies on diatom frustules include the measurement of the silicon isotope composition (δ^{30}Si) of diatom frustules as a proxy for local silicic acid utilization (De la Rocha et al. 1998; De la Rocha 2006; Reynolds et al. 2008; Maier et al. 2013). In addition, the carbon and nitrogen isotopic compositions (δ^{13}C and δ^{15}N) of organic matter occluded within diatom frustules are regarded as proxies for the carbon and nitrogen cycles (Singer and Shemesh 1995; Sigman et al. 1999; Crosta and Shemesh 2002; Studer et al. 2015). However, in most previous studies, geochemical measurement of diatom frustules has been carried out on samples of mixed diatom taxa because the conventional methods (e.g., chemical treatment with hydrogen peroxide [H_2O_2] and hydrochloric acid [HCl]) do not allow isolation of diatom frustules by taxon.

Each diatom taxon has different ecological characteristics (e.g., blooming season and habitat depth); thus, it is necessary to collect diatom frustules by taxon for accurate geochemical analysis of diatoms. In other words, restricting the number of species is essential for obtaining more accurate paleoenvironmental information and avoiding mixed information from various seasons/depths. However, because of the small size of diatom valves (several tens of micrometers), isolation of any taxon by morphological features using conventional methods has been very challenging (cf. hand-picking under a stereomicroscope, which is a widely accepted method for foraminifer-based studies).

In recent years, flow cytometry, in the form of a cell sorter, has been applied to geological samples to isolate target particles, such as micromanganese nodules (Uramoto et al. 2019), diatom fossils (Tennant et al. 2013a; Ijiri et al. 2021), and fossil pollen (Tennant et al. 2013b; Zimmerman et al. 2018; Tunno et al. 2021; Kasai et al. 2021; Yamada et al. 2021). A cell sorter is an instrument that can separate microparticles by their optical characteristics, reflecting the material's size, structure, or chemical composition (fluorescence). Cell sorters were initially used in the life sciences to collect living cells selectively. By focusing on optical scattering, which reflects differences in the size and structure of diatoms, Ijiri et al. (2021) established a method to purify discoid diatoms using a cell sorter. However, purification of other diatom taxa, such as pennate diatoms, has not yet been achieved, and thus far, it has not been possible to isolate diatom frustules by taxon selectively.

By fully utilizing the capability of a cell sorter to distinguish particles by their optical characteristics (i.e., focusing on both scattering and fluorescence signals from particles), we have established a purification method to selectively obtain various diatom taxa with high purity (ca. 85%–100%). This method is based on discovering that diatom frustules of different taxa exhibit distinct optical characteristics (Sect. 3.1). Five diatom taxa were successfully purified in this study: *Thalassiosira* spp., *Fragilariopsis* spp., *Eucampia antarctica*, *Rhizosolenia* spp., and *Thalassiothrix* spp.

2 Methods

2.1 Sediment samples

For the development of the purification method, we used six sediment samples from a sediment core at Hole U1538A, retrieved from the Scotia Sea, Atlantic sector of the Southern Ocean (57° 26.5248′ S, 43° 21.4691′ W; water depth, 3130.58 m; core length, 676.0 m) during the International Ocean Discovery Program (IODP) Expedition 382 (Fig. 1). The studied samples range from 382-U1538A-1-1, 24–25 cm (0.24 m below seafloor [mbsf]) to 382-U1538A-5-6, 24–25 cm (43.42 mbsf). We selected these samples to confirm that the method developed in this study could be applied to various types of sediment. The approximate age of the sediment core was estimated by paleomagnetic/biostratigraphic analysis and from physical properties such as magnetic susceptibility (Weber et al. 2021). The upper two samples (0.24 and 1.73 mbsf) correspond to the Holocene, the middle two (15.10 and 17.54 mbsf) to the last glacial period, and the lower two (42.54 and 43.42 mbsf) to the last interglacial (Fig. 1). The analyzed interval of the sediment core consists of interbedded dark greenish-gray diatom oozes (interglacial periods) with variable terrigenous components and biosilica-rich/bearing silty clays (glacial periods) (Weber et al. 2021).

2.2 Pretreatment of the sediment samples

We pretreated the samples to concentrate the diatom frustules. We followed the pretreatment method of Ijiri et al. (2021), with slight modifications, but omitted the elutriation process (enriching discoid diatoms, which corresponds to "Step 2" of Ijiri et al. 2021) to preserve the diverse diatom taxa in the samples (Fig. 2). Because the elutriation process is time-consuming, its omission markedly reduces the time needed for the pretreatment. In brief, the samples were pretreated as follows (Fig. 2): organic matter and carbonates were removed by 30% H_2O_2 and 5% HCl. The H_2O_2 and HCl treatments were carried out separately (i.e., not with a mixed solution). The samples were sieved through 63, 45, 32, and 20 μm stainless-steel meshes in succession (with the 63 μm sieve being first and the 20 μm sieve being last) to obtain the 20–32 μm fraction. The use of 63 and 45 μm meshes was intended to improve the recovery of the 20–32 μm fraction: if a sediment sample is processed through a 32 μm sieve without pre-sieving, large particles (> 45 μm) clog the mesh so that smaller particles (< 32 μm), which would

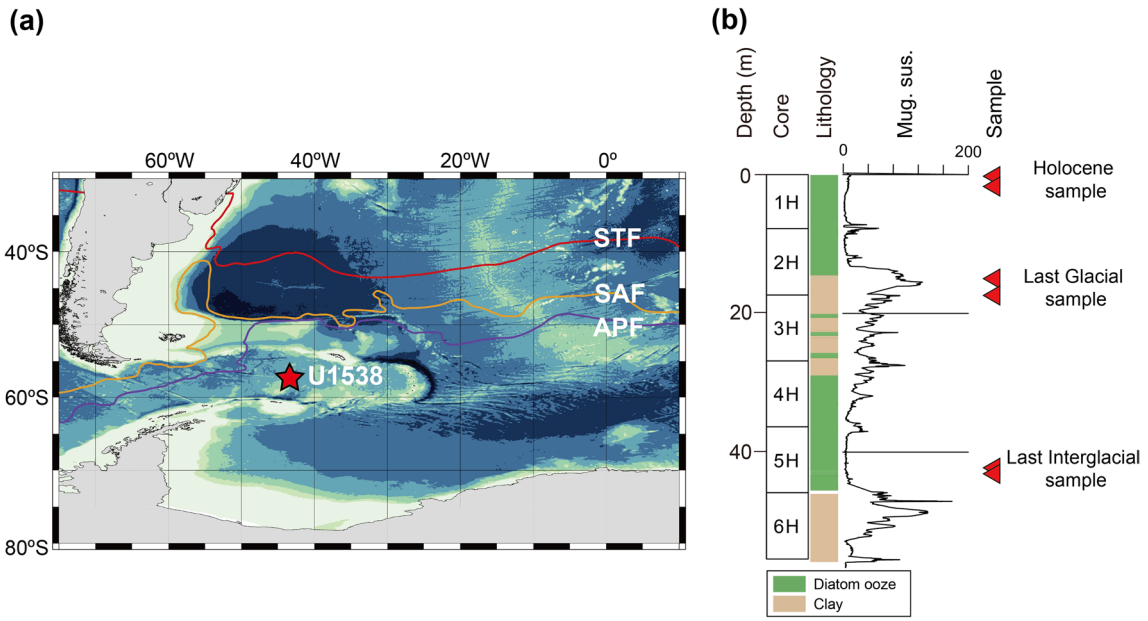

Fig. 1 Location and core profile of the studied samples. **a** Map showing the location of the drilling site (IODP Expedition 382 Site U1538). APF: Antarctic Polar Front, SAF: Subantarctic Front, STF: Subtropical Front. **b** Horizons of the six samples analyzed in this study (red triangles) together with lithology and magnetic susceptibility (Weber et al. 2021)

usually pass through the sieve, also remain on the sieve. The 20–32 μm fraction was selected so that the particles would not jam in the nozzle of the cell sorter (diameter 100 μm). Then clay minerals were removed by heavy-liquid separation using sodium polytungstate (SPT; $3Na_2WO_4{\cdot}9WO_3{\cdot}H_2O$) solution (2.1 g/cm^3) (Morley et al. 2004). Finally, the extracted sample was sieved again through 20 μm mesh to remove any particles that might clog the flow path of the cell sorter.

2.3 Microscopic observation

To determine the optical characteristics of the diatom frustules, we observed the pretreated samples under a fluorescence microscope (BX53) equipped with a mercury lamp (BH2-RFL-T3) and a WIB filter unit (U-MWIB, excitation filter: 460–495 nm, emission filter: > 510 nm) (Olympus, Tokyo, Japan). Approximately 0.2 mL of pretreated sample was picked up in a micropipette and placed on a glass slide. Microscopic observations were carried out at 200 × magnification (Fig. 3).

2.4 Flow cytometry/cell sorter

For the cell sorter experiments for taxon-specific sorting of diatom frustules, we used a Moflo XDP cell sorter (Beckman Coulter, Brea, CA, USA) located at the Kochi Core Center, Japan. The cell sorter collects optical signals from the subject particles, including forward scatter (FSC), side scatter (SSC), and fluorescence signals (Tennant et al. 2013a; Uramoto et al. 2019). The cell sorter has a detector in front of the laser beam (input wavelength: 488 nm), which measures FSC, and several detectors to the side, which measure SSC and fluorescence (Additional file 1: Fig. S1). FSC is a light signal detected along the laser path that is primarily caused by light diffraction around the particles and mainly reflects the size of the particles. SSC is a signal detected at a 90° angle relative to the laser beam. The source of the SSC signal is refraction or reflection from the interface between the laser beam and the particles. The complex structure of diatoms can be reflected in the wide range of SSC signals. In addition to FSC and SSC, the cell sorter detects fluorescence signals from the sample particles. Flow cytometric analysis and sorting with FL1 and FL4 filters to detect fluorescence signals were also carried out, because the fluorescence characteristics of diatom frustules may differ depending on the taxon. The FL1 detector detects a fluorescence signal with a wavelength of 530 nm (full width at half maximum 40 nm), which corresponds to green in visible light, whereas detector FL4 detects a fluorescence signal with a wavelength longer than 740 nm (Additional file 1: Fig. S1). Note that the fluorescence observed by the microscope does not always match the fluorescence observed by the cell sorter. To carry out the experiments under the same device conditions (i.e., to align fluctuation of the laser beam), we used commercial fluorescent beads (Flow-Check Fluorospheres 6605359, Beckman Coulter, Brea, CA, USA) to calibrate the laser and detector settings, which included FSC, SSC, and

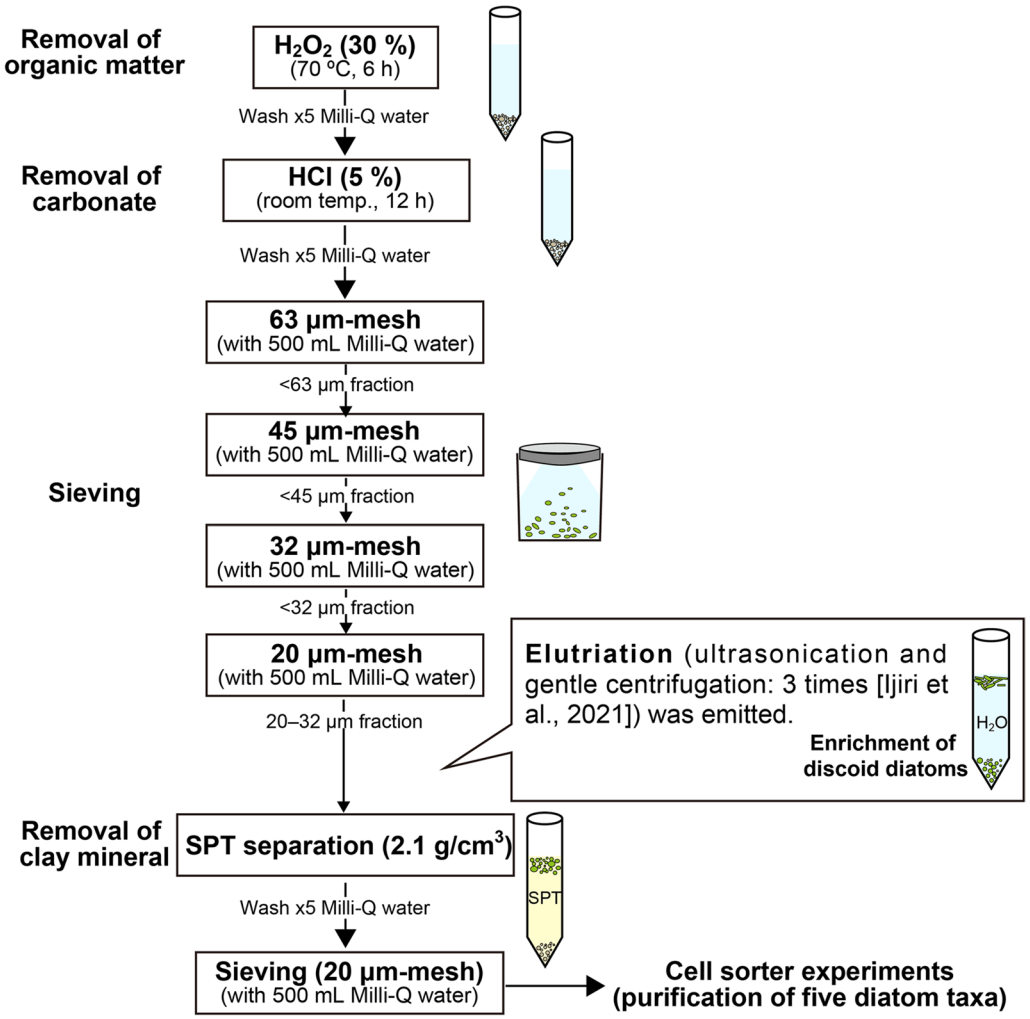

Fig. 2 Flow diagram showing the pretreatment process for concentration of diatom frustules

fluorescence filters. We did not perform any fluorescence correction, a common mathematical method to handle spectral overlap between fluorophores.

The Moflo XDP cell sorter is a "jet-in-air"-type cell sorter in which a water stream is ejected from a narrow nozzle into the air. By diluting the sample suspension so that only one particle passed the laser at a time, we collected optical information on each particle in the suspension. Following Ijiri et al. (2021), we used a solution of 1% NaCl in Milli-Q water for the sheath fluid, and the pretreated sample was suspended in SPT solution (1.1 g/mL) and introduced to the cell sorter. Specific ranges of values can be selected for the optical/fluorescence data, and particles within these ranges are sorted away from the sample stream and collected, leaving the unwanted detritus to be routed to waste. A group of particles to be sorted is specified by an arbitrarily drawn polygon on the sample data, such as the FSC–SSC plot and FL1–FL4 plot (e.g., Fig. 4). The polygon is called a "region." The cell sorter can also sort by combining multiple regions created on multiple data plots; for example, sorting using a region on the FSC–SSC plot, which reflects the optical characteristics of the sample particles (size and internal structure), and a region on the FL1–FL4 plot, which reflects the fluorescence characteristics of the sample particles. This sorting yields particles that satisfy both the desired optical and fluorescence characteristics. A combination of multiple regions is referred to as a "composite region" in this study.

After processing through the cell sorter, the obtained diatom assemblages were analyzed. Microslides for the diatom analyses were prepared using a photocuring adhesive (Nichika Inc., Kyoto, Japan). All diatoms on one microslide were identified at the species level until 50–100 valves had been counted (Additional file 2: Tables S1–S6). We also analyzed strewn slides of

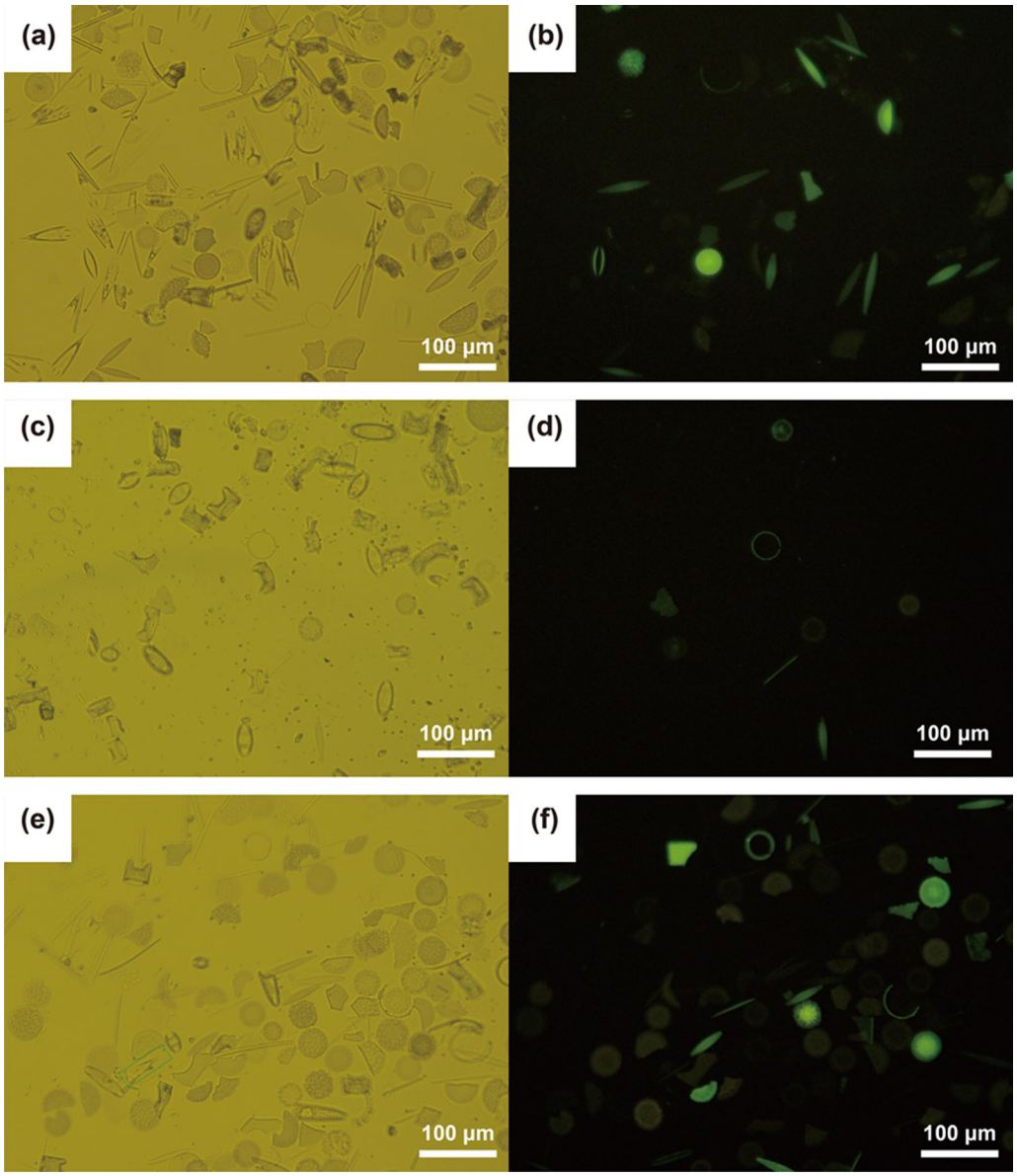

Fig. 3 Photomicrographs of the samples after chemical pretreatment. **a, b** Sample 382-U1538A-1-2, 24–25 cm. **c, d** Sample 382-U1538A-3-1, 24–25 cm. **e, f** Sample 382-U1538A-5-6, 24–25 cm. Images (**a**), (**c**), and (**e**) were taken with transmitted light; images (**b**), (**d**), and (**f**) were obtained by fluorescence imaging

the original sediment samples (i.e., microslides of bulk sediment samples without chemical pretreatment). The original diatom assemblage compositions are presented in Additional file 1: Fig. S2 and Additional file 2: Table S7. A single centric diatom was counted as one when more than half of the valve was observed. A pennate diatom specimen was counted as one when two apices were observed. In addition, the number of fragments of the needle-shaped diatom *Thalassiothrix* (i.e., *Thalassiothrix* specimen without valve apices) on the microslides after the cell sorter experiments was also counted (Additional file 2: Tables S1–S6).

3 Results and discussion

3.1 Sample optical characteristics and cell sorter tuning

We confirmed that the diatom morphologic features, including shape, size, and structure (e.g., the arrangement pattern of areolae), are different among taxa, which created different reflection and scattering patterns in the cell sorter analysis. More importantly, we found that the diatoms sometimes exhibited markedly different

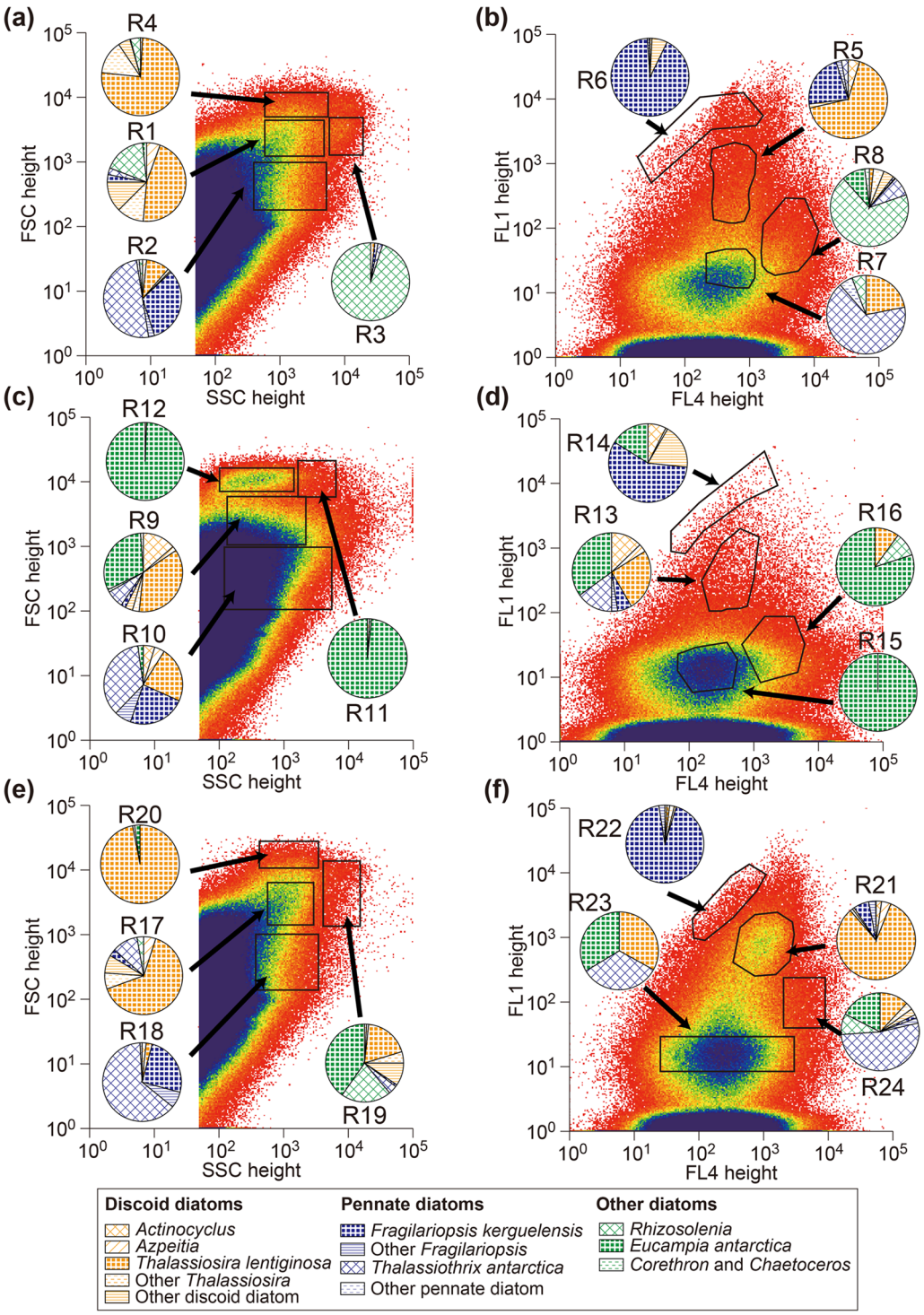

Fig. 4 Flow cytograms and pie charts showing the diatom assemblages obtained from each sorting region. The circled numbers indicate the sorting regions established in this study. **a, b** Sample 382-U1538A-1-2, 24–25 cm (Holocene). **c, d** Sample 382-U1538A-3-1, 24–25 cm (last glacial). **e, f** Sample 382-U1538A-5-6, 24–25 cm (last interglacial). Plots of FSC height versus SSC height are shown in (**a**), (**c**), (**e**), and FL1 height versus FL4 height are shown in (**b**), (**d**), (**f**). Each dot in the flow cytogram indicates a particle that passes through the laser: the bluer the color, the greater the number of particles

Table 1 Summary of the characteristics and diatom assemblages of the sorting regions and composite regions

Description of particle groups	Sorting regions/composite regions	Obtained diatom assemblage
Moderate-FSC	R1/R9/R17	Abundant discoid diatoms (*Thalassiosira*)
Low-FSC	R2/R10/R18	Abundant pennate diatoms (*Fragilariopsis*, *Thalassiothrix* etc.)
High-SSC	R3/R11/R19	Abundant *Rhizosolenia* (interglacial samples) or *Eucampia* (glacial samples)
High-FSC	R4/R12/R20	Increased *Eucampia* (interglacial samples) / Purified *Eucampia* (glacial samples)
Moderate-FL1	R5/R13/R21	Abundant discoid diatoms
High-FL1	R6/R14/R22	Abundant *Fragilariopsis*
Low-FL1	R7/R15/R23	Abundant Thalassiothrix (interglacial samples) / Abundant *Eucampia* (glacial samples)
Low–Mid FL1	R8/R16/R24	Increased *Rhizosolenia*
Moderate-FSC × Moderate-FL1	R1 × R5/R9 × R13/R17 × R21	Purified discoid diatoms, mainly *Thalassiosira*
Low-FSC × High-FL1	R2 × R6/R10 × R14/R18 × R22	Purified *Fragilariopsis*
Low-FSC × Low-FL1	R2 × R7/R10 × R15/R18 × R23	Purified *Thalassiothrix* (interglacial samples)
High-SSC × Low–Mid FL1	R3 × R8/R11 × R16/R19 × R24	Purified *Rhizosolenia* (Holocene samples)

fluorescence features (Fig. 3). Specifically, the genus *Fragilariopsis* showed high fluorescence intensity (visible as bright green in Fig. 3). However, discoid diatoms showed a considerable variation in fluorescence intensity (i.e., the majority of discoid diatoms had far weaker fluorescence intensities than *Fragilariopsis*, but with some exceptions; Fig. 3). In addition, specimens of *Eucampia antarctica* and needle-shaped diatoms (*Thalassiothrix*) showed relatively weak fluorescence intensities (Fig. 3). These observations suggest that the fluorescence characteristics and the morphologic/optical signal are important parameters separating these taxa.

Through many cycles of flow cytometric sorting and microscopic observation, we determined the optical parameters FSC and SSC, which reflect diatom morphology, and the FL1 and FL4 filters, which reflect the fluorescence characteristics of diatom frustules. Because the morphology of diatom frustules was too complex to predict the flow cytometric characteristics from the microscopic observations, we repeated the sorting and observation cycles to build "an empirical rule". After the sorting trials, we identified the sorting regions, shown in Fig. 4 and Additional file 1: Fig. S3 (Regions 1–45; Table 1). As mentioned in Sect. 2.4, these regions specify the group of particles to be sorted. We also conducted sorting experiments using composite regions, in which multiple regions were combined, to obtain particles satisfying specific optical and fluorescence characteristics. The coordinates of the designated sort regions' upper right and lower left points are listed in Additional file 2: Table S8. These parameters vary depending on the instruments' optical alignments and detector settings (such as the voltage applied to the photomultiplier). Even with the same instrument and the same sample, slight differences of optical alignment can produce shifts in the flow cytometer plot; therefore, we adjusted the region settings sample-by-sample, including several rounds of sorting (ca. 50 particles) and checking under the microscope, after which we finalized the sorting region for that sample. Therefore, the position (parameter values) of each finalized region on the plots shown in Fig. 4 differs between samples. Regions occurring in the FSC–SSC plot reflect the particles' optical characteristics, and those in the FL1–FL4 plot reflect fluorescence signals (Fig. 4). Hereinafter, "region" is abbreviated to "R".

3.2 General results of the sorting experiments

Through the cell sorter experiments, which included sorting of each designated region and composite regions, we succeeded in the purification/enrichment of five diatom taxa that represent Southern Ocean assemblages: discoid diatoms (mainly *Thalassiosira*); *Fragilariopsis* (mainly *Fragilariopsis kerguelensis*); *Rhizosolenia*; *Eucampia antarctica*; and needle-shaped diatoms (mainly *Thalassiothrix*) (Figs. 5–7, Additional file 1: Figs. S4–S6). In addition, light microscopic observation showed that almost no "non-diatom particles" were present in the samples after sorting. To confirm the method's applicability to collect these diatom taxa selectively, we sorted the diatoms in each of the six samples in the various regions (Fig. 4 and Additional file 1: Fig. S3). In the following section, the diatom assemblages obtained during the sorting experiments in each region and composite regions are described. Note that the term "relative abundance" indicates the relative frequency of each diatom taxon in the diatom assemblage, not in the total particles.

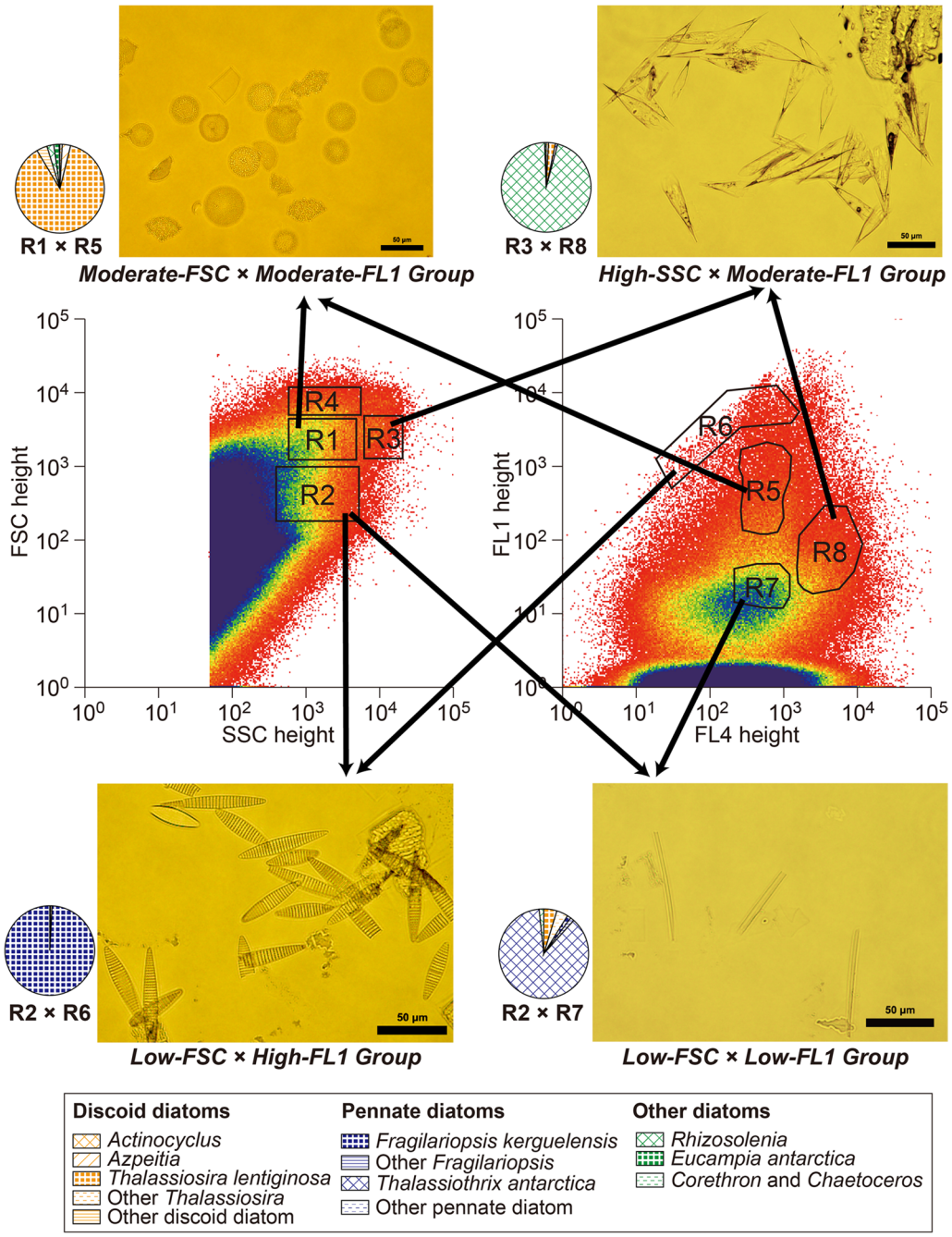

Fig. 5 Flow cytograms of sample 382-U1538A-1-2, 24–25 cm (Holocene) and pie charts/photomicrographs showing the diatom assemblages obtained by sorting of the following composite regions: Regions 1 and 5 (discoid-diatom-rich); Regions 2 and 6 (*Fragilariopsis*-rich); Regions 3 and 8 (*Rhizosolenia*-rich); and Regions 2 and 7 (*Thalassiothrix*-rich). The crystalline materials in the micrographs are NaCl crystals in the sheath fluid

3.3 Diatom assemblages obtained from sample-adjusted sorting regions

In the Holocene sample (U1538A-1-2, 24–25 cm), sorting of R1 (moderate FSC values) yielded a diatom assemblage mainly composed of discoid diatoms (*Thalassiosira*). The relative abundance of this taxon was 75.2% (Fig. 4a). In contrast, the main components of the diatom assemblage obtained from R2 sorting were pennate diatoms such as *Fragilariopsis kerguelensis* (31.9%) and *Thalassiothrix antarctica* (50.0%) (Fig. 4a). R3, from which we obtained a *Rhizosolenia*-dominated assemblage (94.7%), was characterized by higher SSC values (Fig. 4a). We also defined

a region (R4) that had high FSC values, which was mainly composed of discoid diatoms. Of the regions identified in the FL1–FL4 plot, the diatom assemblage obtained by sorting of R5 (with a moderate degree of fluorescence) was composed of discoid diatoms, whereas the main component of the assemblage from R6 (with high FL1 values) was *Fragilariopsis kerguelensis* (Fig. 4b). We also obtained *Thalassiothrix*-rich (needle-shaped diatoms) and *Rhizosolenia*-rich assemblages from sorting of R7 (the lowest FL1 values) and R8 (slightly higher FL1 and FL4 values), respectively (Fig. 4b). In addition, we conducted sorting experiments in composite regions. Specifically, sorting of the composite region R1 × R5 resulted in isolation of discoid diatoms with high purity (relative abundance 95.6%; Fig. 5). Sorting of the composite region R2 × R6 yielded highly pure assemblages of *Fragilariopsis* (relative abundance 99.0%; Fig. 5). We also obtained an assemblage dominated by needle-shaped diatoms (*Thalassiothrix*, relative abundance 86.9%) by sorting the composite region R2 × R7 (Fig. 5). In addition, we succeeded in isolating *Rhizosolenia* with high purity (95.2%) by sorting the composite region R3 × R8 (Fig. 5).

In the last glacial sample (U1538A-3-1, 24–25 cm), we designated eight regions for sorting (R9 to R16; Fig. 4c, d). The diatom assemblage from R9 (moderate FSC values) was composed of discoid diatoms (57.6%) and *Eucampia antarctica* (31.2%) (Fig. 4c). In contrast, R10 (low FSC values) assemblages contained greater relative abundances of pennate diatoms (*Fragilariopsis* 23.8%, *Thalassiothrix* 35.6%) (Fig. 4c). We also obtained *Eucampia*-dominated assemblages from R11 (higher SSC) and R12 (high FSC) (Fig. 4c). In the sorting of R13 (moderate FL1 fluorescence), we recognized an assemblage mainly composed of discoid diatoms and *Eucampia* (Fig. 4d); in contrast, we observed markedly higher abundances of *Fragilariopsis* in the R14 (high FL1) assemblage (Fig. 4d: 57.3%). Both R15 (lowest FL1) and R16 (lower FL1) yielded *Eucampia*-dominated assemblages, although the R16 assemblage contained slightly higher proportions of *Rhizosolenia* (Fig. 4d). In addition, sorting of the composite region R9 × R13 yielded purified discoid diatoms (relative abundance 86.8%; Fig. 6). We also obtained highly pure assemblages of *Fragilariopsis* by sorting the composite region R10 × R14 (relative abundance 97.4%; Fig. 6).

In the last interglacial sample (U1538A-5-6, 24–25 cm), eight sorting regions were defined (R17 to R24). Sorting of R17 (moderate FSC values) yielded abundant discoid diatoms (83.9%; Fig. 4e), whereas sorting of R18 (low FSC values) produced an assemblage dominated by pennate diatoms (*Fragilariopsis* 25.0%, *Thalassiothrix* 63.3%) (Fig. 4e). The assemblage from R19 (high SSC values) showed high proportions of *Rhizosolenia* (20.6%) and *Eucampia* (40.2%) (Fig. 4e). In addition, a discoid-diatom-rich assemblage was obtained from the sorting of R20 (high FSC) (Fig. 4e). For the FL1–FL4 plot, the diatom assemblages of R21 (moderate FL1) and R22 (high FL1) showed very high abundances of discoid diatoms (90.9%) and *Fragilariopsis* (92.6%), respectively (Fig. 4f). The assemblages from R23 (lowest FL1) and R24 (low FL1) were composed of *Thalassiothrix* (needle-shaped diatoms) and *Eucampia* (Fig. 4f). In addition, we obtained purified assemblages of discoid diatoms (96.4%), *Fragilariopsis* (97.9%), and *Thalassiothrix* (90.5%) by sorting experiments of composite regions R17 × R21, R18 × R22, and R18 × R23, respectively (Fig. 7).

3.4 Purification/enrichment of representative diatom taxa

In this section, the regions and composite regions described above are grouped based on the optical characteristics of the particles ("description of particle groups" in Table 1), and the results obtained for each group are compared and described.

R1, R9, and R17 had moderate FSC values (on the order of 10^3), and discoid diatoms comprised the majority of this moderate-FSC group (Fig. 4; Table 1). The relative abundance of discoid diatoms was 57.6–83.9% (Fig. 4), markedly higher than their relative abundances in the original assemblages (Additional file 1: Fig. S2).

R2, R10, and R18 had lower FSC values than the moderate-FSC group (Fig. 4; Table 1). Higher abundances of pennate diatoms characterized this low-FSC group. The relative abundance of *Fragilariopsis* was 23.8–31.9% in the low-FSC group, but was less than 5% in the moderate-FSC group. Apart from *Fragilariopsis*, the low-FSC group contained needle-shaped diatoms such as *Thalassiothrix* (35.6–63.3%) and discoid diatoms (4.2–31.7%) (Fig. 4).

R3, R11, and R19 had higher SSC values than the other regions (Fig. 4; Table 1 and Additional file 2: Table S8). The assemblages of the high-SSC group varied among the samples. In the Holocene sample, the genus *Rhizosolenia* constituted the majority of the high-SSC Group (Fig. 4a). In the last glacial period sample, the high-SSC group was characterized by abundant *Eucampia antarctica* (Fig. 4c); in contrast, the high-SSC group for the last interglacial sample yielded diatom assemblages with ca. 20% *Rhizosolenia* (Fig. 4e). The higher abundance of *Rhizosolenia* in the high-SSC group was consistent with the taxon having a more complex valve structure and morphology than other taxa (e.g., the discoid diatom *Thalassiosira* and the pennate diatom *Fragilariopsis*). The difference in the relative abundance of *Rhizosolenia* in the high-SSC group assemblages seems to be due to differences in the compositions of the original assemblages (i.e., *Rhizosolenia* was

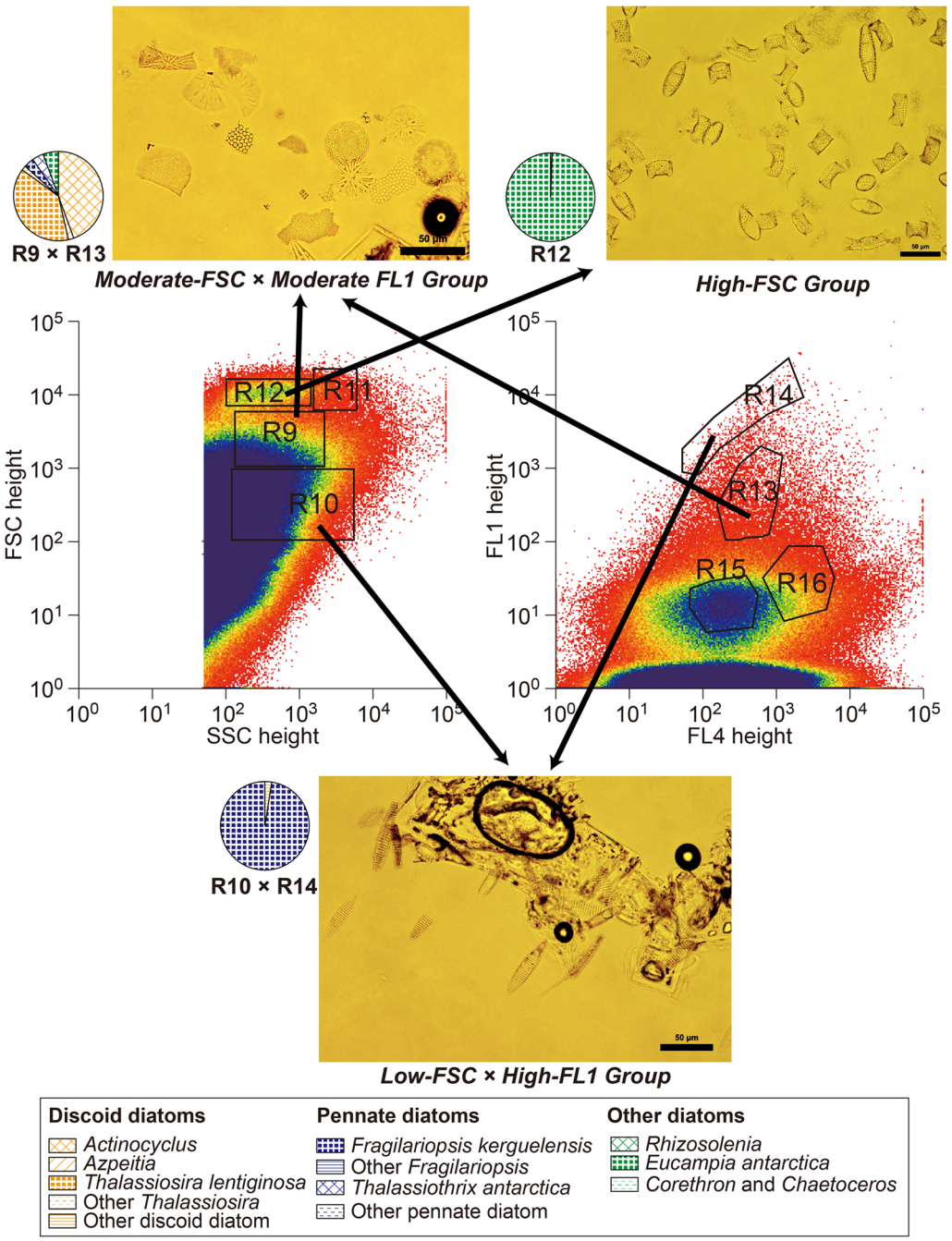

Fig. 6 Flow cytograms of sample 382-U1538A-3-1, 24–25 cm (last glacial) and pie charts/photomicrographs showing the diatom assemblages obtained by sorting of the following composite regions: Regions 9 and 13 (discoid-diatom-rich); Regions 10 and 14 (*Fragilariopsis*-rich); and Region 12 (*Eucampia*-rich). Sorting of composite region R12 and R15 also achieved purification of *Eucampia antarctica* (Additional file 2: Table S4). The crystalline materials in the micrographs are NaCl crystals in the sheath fluid

most abundant in Holocene samples) (Additional file 1: Fig. S2; Additional file 2: Table S7).

R4, R12, and R20 had the highest FSC values (Fig. 4; Table 1). Although the diatom assemblages of this high-FSC group varied greatly among samples, all samples showed an increased percentage of *Eucampia antarctica* relative to the original samples (Fig. 4; Additional file 1: Fig. S2). In the sample from the last glacial, the high-FSC group consisted almost entirely of *Eucampia antarctica* (Figs. 4 and 6).

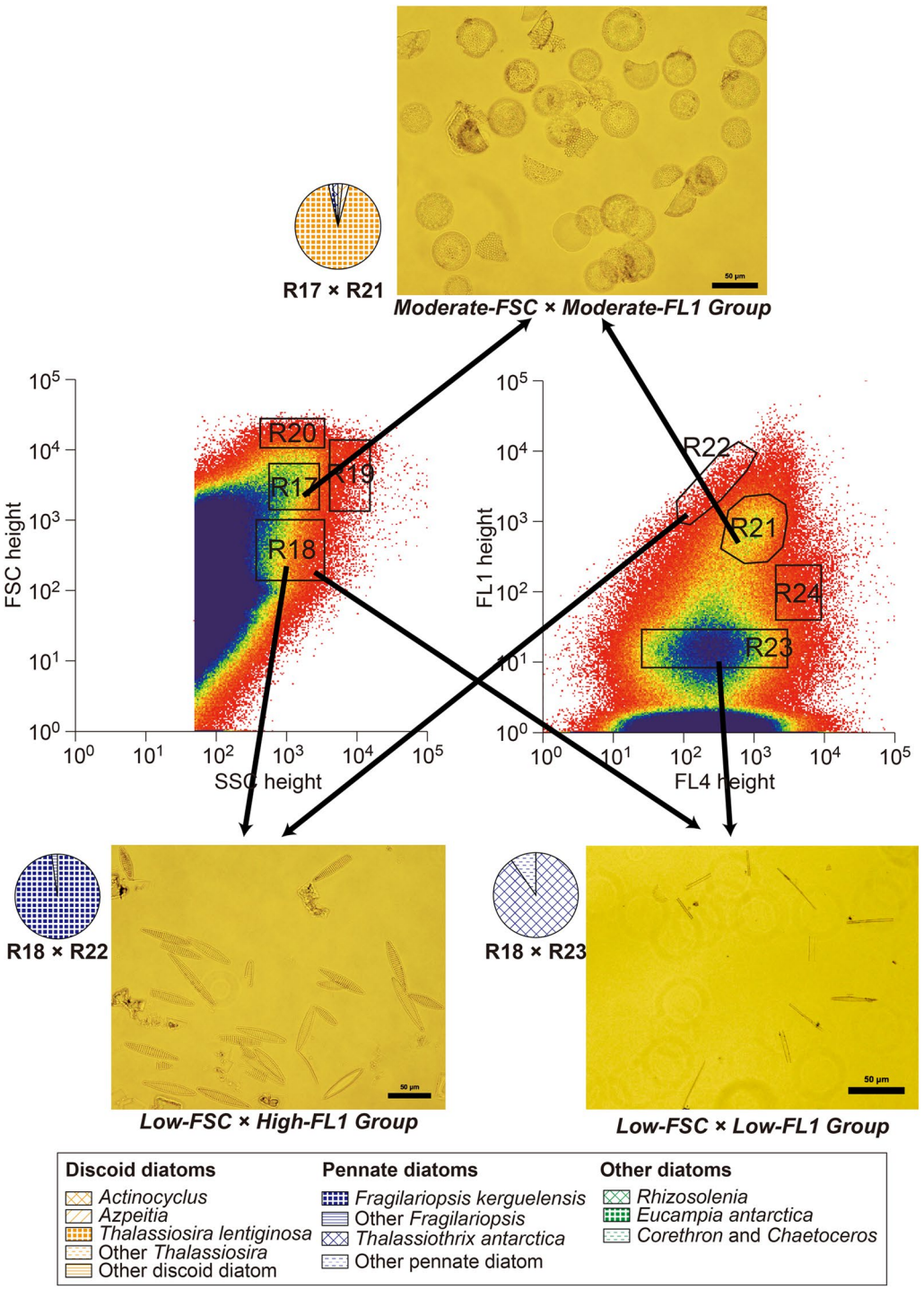

Fig. 7 Flow cytograms of sample 382-U1538A-5-6, 24–25 cm (last interglacial) and pie charts/photomicrographs showing the diatom assemblages obtained by sorting of the following composite regions: Regions 17 and 21 (discoid-diatom-rich); Regions 18 and 22 (*Fragilariopsis*-rich); and Regions 18 and 23 (*Thalassiothrix*-rich). The crystalline materials in the micrographs are NaCl crystals in the sheath fluid

R5, R13, and R21 contained particles that emit moderate fluorescence (Fig. 4b, d, f, Table 1), and this moderate-FL1 group was mainly composed of discoid diatoms (Fig. 4): specifically, the relative abundances of discoid diatoms were ca. 70–90% in the Holocene and last interglacial samples (Fig. 4b, f) and ca. 40% in the last glacial sample (Fig. 4d).

R6, R14, and R22 had the highest FL1 values among the designated sorting regions (Fig. 4; Table 1), meaning that the diatoms of the high-FL1 group emit high fluorescence in the wavelength region 510–550 nm (Additional file 1: Fig. S1), which corresponds to green in visible light (Fig. 3). In all samples, the high-FL1 group was composed mainly of *Fragilariopsis kerguelensis*. This result is consistent with the microscopic observations described in Sect. 3.1 that most of the *Fragilariopsis* spp. specimens showed high fluorescence (i.e., high FL1 values), whereas the fluorescence intensity of discoid diatoms varied (Fig. 3).

Particles in R7, R15, and R23 had relatively lower FL1 values (Fig. 4b, d, f; Table 1). The diatom assemblages of the low-FL1 group varied among samples: needle-shaped diatoms (*Thalassiothrix*) were abundant in the Holocene and last interglacial samples (Fig. 4b, f), whereas *Eucampia antarctica* dominated the R15 assemblage in the last glacial sample (Fig. 4d). This result is consistent with the microscopic observation that *Thalassiothrix* and *Eucampia* emit relatively weak fluorescence (Fig. 3).

Particles in R8, R16, and R24 had relatively higher fluorescence values than the low-FL1 group (Fig. 4; Additional file 2: Tables S1 and S8), and are referred to here as the low–mid FL1 group. The diatom assemblages in the low–mid FL1 group showed higher abundances of *Rhizosolenia* than those from other regions, although the magnitude of the increase varied from sample to sample. Specifically, the Holocene sample yielded a *Rhizosolenia*-rich assemblage (Fig. 4b). In contrast, the last glacial sample was composed mainly of *Eucampia antarctica* (Fig. 4d). The last interglacial sample also showed a slight increase in *Rhizosolenia*; however, needle-shaped diatoms (*Thalassiothrix*) were dominant (Fig. 4f).

As mentioned above, we also conducted sorting experiments using composite regions to obtain particles exhibiting both optical and fluorescence characteristics of interest. Sorting of the moderate-FSC and moderate-FL1 groups (i.e., sorting with composite regions R1 × R5, R9 × R13, and R17 × R21) yielded discoid diatoms with high purity (relative abundance 86.8–96.4%; Figs. 5, 6, 7).

Sorting of composite regions to obtain particles that exhibit low-FSC and high-FL1 characteristics (i.e., composite regions R2 × R6, R10 × R14, and R18 × R22) yielded highly pure assemblages of *Fragilariopsis kerguelensis*, the most abundant diatom taxon in the Southern Ocean (relative abundance 97.4–99.0%; Figs. 5, 6, 7). As described above, *Fragilariopsis*, discoid diatoms, and needle-shaped diatoms were present in variable proportions in the low-FSC group assemblages (R2, R10, and R18; Fig. 4a, c, e). By utilizing the fluorescence characteristics, we selectively sorted *Fragilariopsis kerguelensis* with high purity (Figs. 5, 6, 7) while removing discoid and needle-shaped diatoms that emit relatively weak fluorescence (Fig. 3).

Table 2 Summary of the optical and fluorescence characteristics of the five targeted diatom taxa

Diatom taxa	FSC	SSC	FL1 (fluorescence)
Thalassiosira (discoid diatom)	Mid (~ 10^3)	Mid (~ 10^2–10^3)	Mid (~ 10^2–10^3)
Fragilariopsis	Low (~ 10^2)	Mid (~ 10^2–10^3)	High (~ 10^3–10^4)
Rhizosolenia	High (~ 10^4)	High (~ 10^4)	Low (~ 10^1–10^2)
Eucampia	High (~ 10^4)	Mid (~ 10^2–10^3)	Low (~ 10^1–10^2)
Thalassiothrix (needle-shaped diatom)	Low (~ 10^2)	Mid (~ 10^2–10^3)	Low (~ 10^1–10^2)

For the Holocene and last interglacial samples, we obtained highly pure assemblages of needle-shaped diatoms (*Thalassiothrix*, relative abundance ca. 90%) by sorting the composite regions to obtain particles with both low FSC and low FL1 (i.e., composite regions R2 × R7 and R18 × R23) (Figs. 5 and 7). Thus, application of fluorescence characteristics allowed us to remove other pennate and discoid diatoms from the low-FSC group assemblages (R2 and R18) and purify needle-shaped diatoms. In addition, for the Holocene sample, we succeeded in isolating *Rhizosolenia* with high purity (95.2%) by sorting particles that satisfy the characteristics of both high-SSC and low–mid-FL1 group with the composite region R3 × R8 (Fig. 5).

In summary, we succeeded in purifying five diatom taxa that are major components of the Southern Ocean diatom flora and confirmed the applicability of this new purification protocol through cell sorter experiments on six samples (Figs. 5, 6, 7 and Additional file 1: Figs. S3–S5, Tables 1 and 2 and Additional file 2: Tables S1–S6). Specifically: (1) discoid diatoms were purified using composite regions to sort particles with both moderate FSC and moderate FL1 values; (2) purification of *Fragilariopsis* (mainly *Fragilariopsis kerguelensis*) was achieved by sorting the composite regions of low FSC and high FL1; (3) sorting of the composite regions with both high SSC and low–mid FL1 yielded *Rhizosolenia*-dominated assemblages from the Holocene samples; (4) sorting of high-FSC group particles yielded purified *Eucampia antarctica* from the glacial samples; and (5) sorting composite regions to obtain low-FSC and low-FL1 particles

achieved purification of needle-shaped diatoms (*Thalassiothrix*) from the interglacial samples.

3.5 Implications

We established a taxon-specific diatom purification method using conventional pretreatments and a cell sorter. The improvements in this study relative to the previous method of Ijiri et al. (2021) are: (1) the new method is more straightforward, with one fewer pretreatment step (omission of the elutriation process); and (2) the new method can selectively isolate a variety of taxa, in contrast to the previous method that could isolate only discoid diatoms.

The purification method established in this study has many potential applications. First, it contributes to paleoceanography, especially in high-latitude and upwelling regions where diatoms are abundant. Purification of selected diatom taxon will enable measurement of geochemical proxies such as $\delta^{18}O$, $\delta^{31}Si$, $\delta^{13}C$, and $\delta^{15}N$ of diatom frustules more accurately, removing biases caused by differences in the ecological preferences of each taxon.

This method can also be applied to improve efficiency in various studies involving morphological analysis of selected diatom taxa. For example, several attempts have used morphological variations of diatom taxa such as *Fragilariopsis kerguelensis* and *Eucampia antarctica* as paleoenvironmental indicators to reconstruct oceanic fronts, sea-surface temperature, or sea-ice distribution in the geological past (Kaczmarska et al. 1993; Cortese and Gersonde 2007; Cortese et al. 2012; Allen 2014; Kloster et al. 2018, 2019). By using the new method to enrich a target diatom taxon and then mounting the specimens on a microslide, the time required for microscopic observation (to find and analyze the target taxon under the microscope) can be drastically reduced, especially when the targeted diatom is scarce in samples.

It is also worth emphasizing that the new method successfully purifies *Rhizosolenia* and *Thalassiothrix*. These taxa are the main contributors to primary/export production during summer blooming seasons in the pelagic and coastal oceans (Kemp et al. 2000, 2010); thus, further research using the new method will yield insights into a new aspect of biogeochemical cycles.

Moreover, the method can be extended to other research fields. Possible applications include the extraction of target diatom taxa from living samples for isolating and culturing. In addition, the method would allow non-experts to obtain rough estimations of assemblage compositions because flow cytometric data show the relative abundances of the target particles (Fig. 4; Additional file 2: Table S8). For example, a higher relative abundance of *Eucampia antarctica* can be inferred from the higher density of particles in the high-FSC group (cf. R12 in Fig. 4c). A prominent peak (i.e., high particle density) of the high-FSC group in a glacial sample (Fig. 6) is consistent with the high abundance of *Eucampia antarctica* in the original sample (Additional file 1: Fig. S2; Additional file 2: Table S7).

4 Conclusions

Taxon-specific purification of diatoms is crucial for accurate geochemical analysis of diatom frustules; however, owing to the small size of diatoms, taxon-by-taxon purification has not been achieved so far. In the present study, we developed a purification method for various diatom taxa that uses a cell sorter. After pretreatment (removal of organic matter, carbonates, and clay minerals, followed by sieving), we conducted many cycles of sorting focusing on both optical characteristics (FSC and SSC) and fluorescence characteristics (FL1 and FL4 filters). We selectively sorted five diatom taxa with high purity (ca. 85–100%). Specifically, (1) discoid diatoms were purified using composite regions to sort particles with both moderate FSC and moderate FL1 values; (2) purification of *Fragilariopsis* specimens (mainly *Fragilariopsis kerguelensis*) was achieved by sorting the composite regions with low FSC and high FL1; (3) sorting of the composite regions that satisfy high SSC and low–mid FL1 characteristics extracted *Rhizosolenia* with high purity; (4) high-FSC group particles consisted of purified *Eucampia antarctica*; and (5) sorting of composite regions to obtain low-FSC and low-FL1 particles achieved purification of needle-shaped diatoms (*Thalassiothrix*) (Figs. 5, 6, 7 and Additional file 1: Figs. S3–S5, Additional file 2: Tables S1–S6). Establishing a diatom purification method allows "taxon-specific analysis" in various research fields such as paleoceanography, paleolimnology, ocean biology, and phycology. One example of an impact of this work is improved accuracy of geochemical analysis of diatom frustules, leading to the advancement of paleoceanography, especially for high-latitude and upwelling regions where diatoms are abundant.

Abbreviations

$\delta^{13}C$	Carbon isotopic composition
$\delta^{15}N$	Nitrogen isotopic composition
$\delta^{18}O$	Oxygen isotopic composition
$\delta^{30}Si$	Silicon isotopic composition
FSC	Forward scatter
IODP	International Ocean Discovery Program
JAMSTEC	Japan Agency for Marine-Earth Science and Technology
J-DESC	Japan Drilling Earth Science Consortium
mbsf	Meter below seafloor
SPT	Sodium polytungstate
SSC	Side scatter
X-Star	Institute for Extra-cutting-edge Science and Technology Avant-garde Research

Supplementary Information

The online version contains supplementary material available at https://doi.org/10.1186/s40645-023-00543-5.

Additional file 1. Supplementary Figures S1–S6. Optical path of the cell sorter used in this study (**Figure S1**); Original diatom assemblages of the samples (**Figure S2**); Flow cytograms of samples and pie charts showing the diatom assemblages obtained from each designated region (**Figure S3**); Flow cytograms and pie charts/photomicrographs showing the diatom assemblages obtained by sorting of composite regions (**Figure S4–S6**) (PDF).

Additional file 2. Supplementary Tables S1–S8. Raw data on the diatom assemblages (**Tables S1–S7**); Coordinates of the designated sorting regions (**Table S8**) (Excel).

Acknowledgements
We thank the officers, crew, and scientific party of cruise IODP Expedition 382 (R/V JOIDES Resolution) for sample retrieval and technical support. We are very grateful to Ms. Momoyo Odani (Kochi University) and Ms. Harumi Isshiki (JAMSTEC) for their technical assistance. We also thank Mr. Takeshi Izumi (Kochi University) and Dr. Fumiaki Mori (JAMSTEC) for encouraging discussion throughout the study. This manuscript was greatly improved by constructive comments from the reviewers.

Authors' information
YK's previous affiliation was Kochi University (Center for Advanced Marine Core Research). Portions of the experiments relevant to this paper were performed while YK was affiliated with his former institution.

Author contributions
YK conceived and designed the study, and carried out the entire experiment. YM co-designed the study, analyzed and defined the sorting regions for the cell sorter. AI helped to interpret the data. TT supported the operation of the cell sorter. MI collaborated with the corresponding author in the construction of the manuscript. All authors read and approved the final manuscript.

Funding
This work was supported by JSPS KAKENHI Grant Numbers 19J01441, 20H04973, and 21K14030 (YK), and 17H06318 (AI and MI). The first author (YK) also obtained a travel grant for participation in the scientific cruise IODP Expedition 382 from the Japan Drilling Earth Science Consortium (J-DESC).

Availability of data and materials
Supporting datasets and information for this article are available in the additional files 1 and 2.

Declarations

Competing interests
The authors declare that they have no competing interest.

Received: 12 May 2022 Accepted: 21 February 2023
Published online: 08 March 2023

References

Allen CS (2014) Proxy development: a new facet of morphological diversity in the marine diatom *Eucampia antarctica* (Castracane) Mangin. J Micropalaeontol 33:131–142. https://doi.org/10.1144/jmpaleo2013-025

Cortese G, Gersonde R (2007) Morphometric variability in the diatom *Fragilariopsis kerguelensis*: implications for Southern Ocean paleoceanography. Earth Planet Sci Lett 257:526–544. https://doi.org/10.1016/j.epsl.2007.03.021

Cortese G, Gersonde R, Maschner K, Medley P (2012) Glacial-interglacial size variability in the diatom *Fragilariopsis kerguelensis*: Possible iron/dust controls? Paleoceanography 27:PA1208. https://doi.org/10.1029/2011pa002187

Crosta X, Shemesh A (2002) Reconciling down core anticorrelation of diatom carbon and nitrogen isotopic ratios from the Southern Ocean. Paleoceanography 17:1010. https://doi.org/10.1029/2000PA000565

De la Rocha CL (2006) Opal-based isotopic proxies of paleoenvironmental conditions. Global Biogeochem Cycles 20:GB4S09. https://doi.org/10.1029/2005GB002664

De la Rocha CL, Brzezinski MA, DeNiro MJ, Shemesh A (1998) Silicon-isotope composition of diatoms as an indicator of past oceanic change. Nature 395:680–683. https://doi.org/10.1038/27174

Dutkiewicz A, O'Callaghan S, Müller RD (2016) Controls on the distribution of deep-sea sediments. Geochem Geophys Geosystems 17:3075–3098

Hodell DA, Kanfoush SL, Shemesh A, Crosta X, Charles CD, Guilderson TP (2001) Abrupt cooling of Antarctic surface waters and sea ice expansion in the South Atlantic sector of the Southern Ocean at 5000 cal yr B.P. Quat Res 56:191–198. https://doi.org/10.1006/qres.2001.2252

Ijiri A, Izumi T, Morono Y, Kato Y, Terada T, Ikehara M (2021) Purification of disc-shaped diatoms from Southern Ocean sediment by cell sorter to obtain accurate oxygen isotope record. ACS Earth Space Chem 5:2792–2806. https://doi.org/10.1021/acsearthspacechem.1c00201

Juillet-Leclerc A, Labeyrie L (1987) Temperature dependence of the oxygen isotopic fractionation between diatom silica and water. Earth Planet Sci Lett 84:69–74. https://doi.org/10.1016/0012-821X(87)90177-4

Kaczmarska I, Barbrick NE, Ehrman JM, Cant GP (1993) *Eucampia* Index as an indicator of the Late Pleistocene oscillations of the winter sea-ice extent at the ODP Leg 119 Site 745B at the Kerguelen Plateau. Hydrobiologia 269(270):103–112

Kasai Y, Leipe C, Saito M, Kitagawa H, Lauterbach S, Brauer A, Tarasov P, Goslar T, Arai F, Sakuma S (2021) Breakthrough in purification of fossil pollen for dating of sediments by a new large-particle on-chip sorter. Sci Adv 7:eabe7327. https://doi.org/10.1126/sciadv.abe7327

Kemp AES, Pike J, Pearce RB, Lange CB (2000) The "Fall dump"—a new perspective on the role of a "shade flora" in the annual cycle of diatom production and export flux. Deep-Sea Res II 47:2199–2154. https://doi.org/10.1016/S0967-0645(00)00019-9

Kemp AES, Grigorov I, Pearce RB, Naveira Garabato AC (2010) Migration of the Antarctic Polar Front through the mid-Pleistocene transition: evidence and climatic implications. Quat Sci Rev 29:1993–2009. https://doi.org/10.1016/j.quascirev.2010.04.027

Kloster M, Kauer G, Esper O, Fuchs N, Beszteri B (2018) Morphometry of the diatom *Fragilariopsis kerguelensis* from Southern Ocean sediment: high-throughput measurements show second morphotype occurring during glacials. Mar Micropaleontol 143:70–79. https://doi.org/10.1016/j.marmicro.2018.07.002

Kloster M, Rigual-Hernández A, Armand LK, Kauer G, Trull TW, Beszteri B (2019) Temporal changes in size distributions of the Southern Ocean diatom *Fragilariopsis kerguelensis* through high-throughput microscopy of sediment trap samples. Diatom Res 34:133–147. https://doi.org/10.1080/0269249X.2019.1626770

Labeyrie LD (1974) New approach to surface seawater paleotemperatures using $^{18}O/^{16}O$ ratios in silica of diatom frustules. Nature 248:40–42

Maier E, Chapligin B, Abelmann A, Gersonde R, Esper O, Ren J, Friedrichsen H, Meyer H, Tiedemann R (2013) Combined oxygen and silicon isotope analysis of diatom silica from a deglacial subarctic Pacific record. J Quat Sci 28:571–581. https://doi.org/10.1002/jqs.2649

Morley DW, Leng MJ, Mackay AW, Sloane HJ, Rioual P, Battarbee RW (2004) Cleaning of lake sediment samples for diatom oxygen isotope analysis. J Paleolimnol 31:391–401. https://doi.org/10.1023/B:JOPL.0000021854.70714.6b

Reynolds BC, Frank M, Halliday AN (2008) Evidence for a major change in silicon cycling in the subarctic North Pacific a 2.73 Ma. Paleoceanography 23:PA4219. https://doi.org/10.1029/2007PA001563

Shemesh A, Charles CD, Fairbanks RG (1992) Oxygen isotopes in biogenic silica: global changes in ocean temperature and isotopic composition. Science 256:1434–1436. https://doi.org/10.1126/science.256.5062.1434

Shemesh A, Burckle LH, Hays JD (1995) Late Pleistocene oxygen isotope records of biogenic silica from the Atlantic sector of the Southern Ocean. Paleoceanography 10:179–196. https://doi.org/10.1029/94PĂ0

Shemesh A, Hodell D, Crosta C, Kanfoush S, Charles T, Guilderson T (2002) Sequence of events during the last deglaciation in Southern Ocean

sediments and Antarctic ice cores. Paleoceanography 17:1056. https://doi.org/10.1029/2000PA000599
Sigman DM, Altabet MA, Francois R, McCorkle DC, Gaillard J-F (1999) The isotopic composition of diatom-bound nitrogen in Southern Ocean sediments. Paleoceanography 14:118–134. https://doi.org/10.1029/1998PA900018
Singer AJ, Shemesh A (1995) Climatically linked carbon isotope variation during the past 430,000 years in Southern Ocean sediments. Paleoceanography 10:171–177. https://doi.org/10.1029/94PA03319
Smol JP, Stoermer EF (eds) (2010) The diatoms: applications for the environmental and earth sciences, 2nd edn. Cambridge University Press, Cambridge
Studer AS, Sigman DM, Martínez-García A, Benz V, Winckler G, Kuhn G, Esper O, Lamy F, Jaccard SL, Wacker L, Oleynik S, Gersonde R, Haug GH (2015) Antarctic Zone nutrient conditions during the last two glacial cycles. Paleoceanography 30:845–862. https://doi.org/10.1002/2014PA002745
Swann GEA, Leng MJA (2009) Review of diatom $\delta^{18}O$ in palaeoceanography. Quat Sci Rev 28:384–398. https://doi.org/10.1016/j.quascirev.2008.11.002
Swann GEA, Maslin MA, Leng MJ, Sloane HJ, Haug GH (2006) Diatom $\delta^{18}O$ evidence for the development of the modern halocline system in the subarctic northwest Pacific at the onset of major Northern Hemisphere glaciation. Paleoceanography 21:PA1009. https://doi.org/10.1029/2005PA001147
Tennant RK, Richard TJ, Love J, Lee R (2013a) A new flow cytometry method enabling rapid purification of diatoms from silica-rich lacustrine sediments. J Paleolimnol 49:305–309
Tennant RK, Richard TJ, Brock F, Cook C, Turney CSM, Love J, Lee R (2013b) A new flow cytometry method enabling rapid purification of fossil pollen from terrestrial sediments for AMS radiocarbon dating. J Quat Sci 28:229–236. https://doi.org/10.1002/jqs.2606
Tunno I, Zimmerman SRH, Brown TA, Hassel CA (2021) An improved method for extracting, sorting, and AMS dating of pollen concentrates from lake sediment. Front Ecol Evol 9:668676. https://doi.org/10.3389/fevo.2021.668676
Uramoto G, Morono Y, Tomioka N, Wakaki S, Nakada R, Wagai R, Uesugi K, Takeuchi A, Hoshino M, Suzuki Y, Shiraishi F, Mitsunobu S, Suga H, Takeichi Y, Takahashi Y, Inagaki F (2019) Significant contribution of subseafloor microparticles to the global manganese budget. Nat Commun 10:1–10. https://doi.org/10.1038/s41467-019-08347-2
Weber ME, Raymo ME, Peck VL, Williams T, Armbrecht LH, Bailey I, Brachfeld SA, Cardillo, FG, Du Z, Fauth G, García M, Glüder A, Guitard ME, Gutjahr M, Hemming SR, Hernández-Almeida I, Hoem FS, Hwang J-H, Iizuka M, Kato Y, Kenlee B, Martos YM, O'Connell S, Pérez, LF, Reilly BT, Ronge TA, Seki O, Tauxe L, Tripathi S, Warnock JP, Zheng X (2021) Site U1538. In: Weber ME, Raymo ME, Peck VL, Williams T, the Expedition 382 Scientists (eds) Proceedings of the International Ocean Discovery Program, vol 382. p 48. doi:https://doi.org/10.14379/iodp.proc.382.107.2021.
Yamada K, Omori T, Kitaba I, Hori T, Nakagawa T (2021) Extraction method for fossil pollen grains using a cell sorter suitable for routine ^{14}C dating. Quat Sci Rev 272:107236. https://doi.org/10.1016/j.quascirev.2021.107236
Zimmerman SRH, Brown TA, Hassel C, Heck J (2018) Testing pollen sorted by flow cytometry as the basis for high-resolution lacustrine chronologies. Radiocarbon 61:359–374. https://doi.org/10.1017/RDC.2018.89

Publisher's Note